Preparation of new superconductors by metal doping of two-dimensional layered materials using ethylenediamine

Xiao Miao,[1] Takahiro Terao,[1] Xiaofan Yang,[1] Saki Nishiyama,[1] Takafumi Miyazaki,[2] Hidenori Goto,[1] Yoshihiro Iwasa,[3] and Yoshihiro Kubozono[1,*]

[1]*Research Institute for Interdisciplinary Science, Okayama University, Okayama 700-8530, Japan*

[2]*Research Laboratory for Surface Science, Okayama University, Okayama 700-8530, Japan*

[3]*Department of Applied Physics, The University of Tokyo, Tokyo 113-8656, Japan*

(Received 13 April 2017; published 5 July 2017)

We have studied new superconductors prepared by metal doping of two-dimensional (2D) layered materials, FeSe and $FeSe_{0.5}Te_{0.5}$, using ethylenediamine (EDA). The superconducting transition temperatures (T_cs) of metal-doped FeSe and metal-doped $FeSe_{0.5}Te_{0.5}$, i.e., $(EDA)_yM_xFeSe$ and $(EDA)_yM_xFeSe_{0.5}Te_{0.5}$ (M: Li, Na, and K), were 31–45 K and 19–25 K, respectively. The stoichiometry of each sample was clarified by energy dispersive x-ray (EDX) spectroscopy, and the x-ray powder diffraction pattern indicated a large expansion of lattice constant c, indicating the cointercalation of metal atoms and EDA. The pressure dependence of superconductivity in $(EDA)_yNa_xFeSe_{0.5}Te_{0.5}$ has been investigated at a pressure of 0–0.8 GPa, showing negative pressure dependence in the same manner as $(NH_3)_yNa_xFeSe_{0.5}Te_{0.5}$. The T_c-c phase diagrams of M_xFeSe and $M_xFeSe_{0.5}Te_{0.5}$ were drawn afresh from the T_c and c of $(EDA)_yM_xFeSe$ and $(EDA)_yM_xFeSe_{0.5}Te_{0.5}$, showing that the T_c increases with increasing c but that extreme expansion of c reverses the T_c trend.

DOI: 10.1103/PhysRevB.96.014502

I. INTRODUCTION

During the past decade, many superconducting two-dimensional (2D) layered materials have been fabricated [1–20]. The most significant and exciting materials are probably the families of iron pnictides (FeAs) [1–5] and iron chalcogenides (FeSe) [6–14] because these materials have provided a very fruitful stage for research on superconductivity. The highest superconducting transition temperatures (T_cs) in these materials are currently recorded for $SmFeAsO_{1-\delta}$ [5] and for $(NH_3)_yNa_xFeSe$ [9]. The highest T_c of the former material is 55 K and that of the latter is 45 K. Here, it should be noted that the T_c of FeSe is at most 8 K [6], but it increases rapidly to 31 K [7] with K doping. Clearly, metal doping is an effective way to produce high T_c superconductors using FeSe-based materials. Furthermore, metal-doped FeSe prepared using ammonia (NH_3), $(NH_3)_yM_xFeSe$ (M: alkali and alkali-earth metal atoms) [9–14], provided a higher T_c than nonammoniated metal-doped FeSe [7,8]. These results show the effectiveness of codoping of FeSe with a metal atom and NH_3.

Recently, we observed a very high T_c in $(NH_3)_yCs_xFeSe$ under high pressure, i.e., the T_c reached 49 K at 21 GPa [13]. This is the highest T_c yet reported in FeSe materials; nonammoniated K_xFeSe also formed a pressure-induced high-T_c phase (T_c = 48.7 K at 12.5 GPa) [8]. Thus, metal-doped FeSe has attractive physical properties. On the other hand, the T_c of $(NH_3)_yCs_xFeSe$ decreased monotonically with increasing pressure up to 13 GPa [13]. The T_c was correlated with the lattice constant, c, i.e., the FeSe plane spacing [13], with the correlation supported not only by the effect of physical pressure but also by the chemical pressure when metal atoms of different sizes were intercalated in FeSe using liquid NH_3 [9–12]. This implies that higher T_cs were the result of larger FeSe plane spacing. Nevertheless, the extreme expansion of FeSe plane spacing suppressed the T_c in FeSe material [15–17]. However, this behavior has not yet been confirmed for $FeSe_{0.5}Te_{0.5}$ because of a lack of data for $FeSe_{0.5}Te_{0.5}$ crystals with extremely expanded layer spacing.

In this paper, we have succeeded in the preparation of metal-doped $FeSe_{0.5}Te_{0.5}$ using ethylenediamine [EDA ($C_2H_8N_2$)] instead of liquid NH_3 and in experimentally obtaining the correlation between T_c and c over a wide c range. The molecular structure of EDA is shown in Fig. 1. There are many advantages of using EDA in metal doping. First, EDA is liquid at room temperature, while NH_3 is liquid below ~240 K, making sample preparation with EDA easier than with liquid NH_3. Furthermore, a larger 2D layer spacing can be realized through the codoping of metal atoms and EDA because the van der Waals size of EDA is much larger than that of NH_3. In this paper, various metal-doped FeSe and $FeSe_{0.5}Te_{0.5}$ samples prepared using EDA are characterized by magnetic susceptibility (M/H), EDX spectroscopy, and x-ray diffraction (XRD); M and H refer to magnetization and applied magnetic field, respectively. The T_c-c phase diagram was obtained for metal-doped FeSe and $FeSe_{0.5}Te_{0.5}$ over a wide c range. Furthermore, the pressure dependence of superconductivity in metal-doped $FeSe_{0.5}Te_{0.5}$ was also investigated to determine the behavior of T_c against pressure in the low-pressure range because this may differ depending on the solvent molecule codoped with the metal atoms.

II. EXPERIMENTAL

The β-FeSe and β-$FeSe_{0.5}Te_{0.5}$ samples were prepared using the method described in Ref. [10]; the prepared samples were identified as $Fe_{0.867(1)}Se$ and $Fe_{0.852(1)}Se_{0.547(1)}Te_{0.45(4)}$ using EDX spectroscopy, which will be described later. The samples of $(EDA)_yM_xFeSe_{1-z}Te_z$ (M = metal atom: Li, Na, and K; z = 0 and 0.5) were prepared using EDA as described below. (1) The metal was immersed together with $Fe_{0.867(1)}Se$ or $Fe_{0.852(1)}Se_{0.547(1)}Te_{0.45(4)}$ in dried EDA solvent.

*Corresponding author: kubozono@cc.okayama-u.ac.jp

 ©2017 American Physical Society

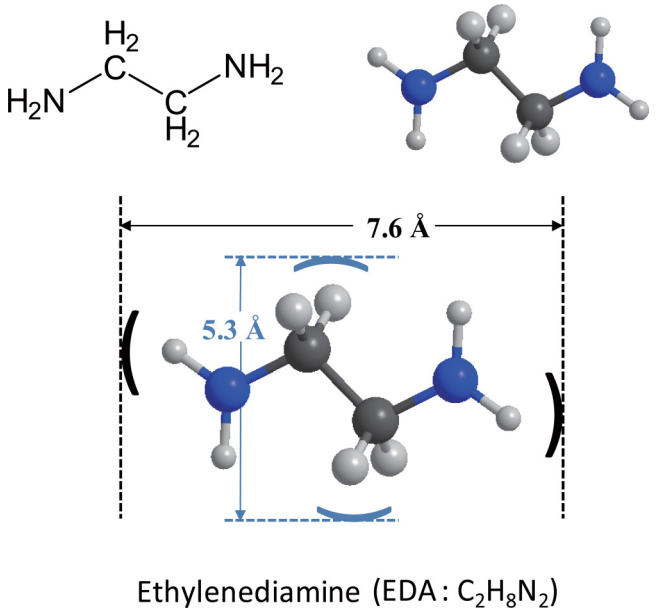

FIG. 1. Molecular structure of EDA. The van der Waals size of EDA is also shown.

The metal was completely dissolved, but $Fe_{0.867(1)}Se$ and $Fe_{0.852(1)}Se_{0.547(1)}Te_{0.45(4)}$ were not dissolved. (2) The solution was stirred at 318 K for one week in an O_2- and H_2O-free glove box (O_2,H_2O < 1.0 ppm). (3) Solvent was removed under vacuum, and the solid sample was introduced into the measurement cell for each characterization.

The M of the sample was measured using a SQUID magnetometer (Quantum Design MPMS2). The T_c and shielding fraction were 9 K and 82% at 2.5 K for $Fe_{0.867(1)}Se$, while they were 14.0 K and 100% at 2.5 K for $Fe_{0.852(1)}Se_{0.547(1)}Te_{0.45(4)}$. The x-ray powder diffraction patterns of the samples were measured with a Rigaku R-Axis Rapid-NR x-ray diffractometer with a Mo Kα source (wavelength $\lambda = 0.71073$ Å). The chemical composition of each sample was determined by EDX spectroscopy with an EDX spectrometer equipped with a scanning electron microscope (Keyence VE-9800/EDAX Genesis XM_2). Throughout this paper, the stoichiometry of the samples is initially provided as the nominal experimental value, as in FeSe and $FeSe_{0.5}Te_{0.5}$, without an estimated standard deviation (esd), and the exact stoichiometry as determined from the EDX spectrum is also given with esd for all samples.

III. RESULTS AND DISCUSSION

The M/H-T plots measured in zero field cooled (ZFC) and field cooled (FC) modes for $(EDA)_yNa_xFeSe$ prepared by the intercalation of Na atoms in FeSe using EDA are shown in Fig. 2(a). A drop in M/H is observed below 44 K (or $T_c^{onset} = 44$ K), and T_c is 43 K. The T_c of this superconducting phase is similar to the T_c(=46 K) of the high-T_c phase of $(NH_3)_yNa_xFeSe$ [12]; $(NH_3)_yNa_xFeSe$ has two different superconducting phases ($T_c = 46$ K and $T_c = 33$ K). The shielding fraction of the $(EDA)_yNa_xFeSe$ sample ($T_c = 43$ K) was evaluated to be 25% at 5 K from the M/H-T plot shown in Fig. 2(a). The superconducting $(EDA)_yNa_xFeSe$ with

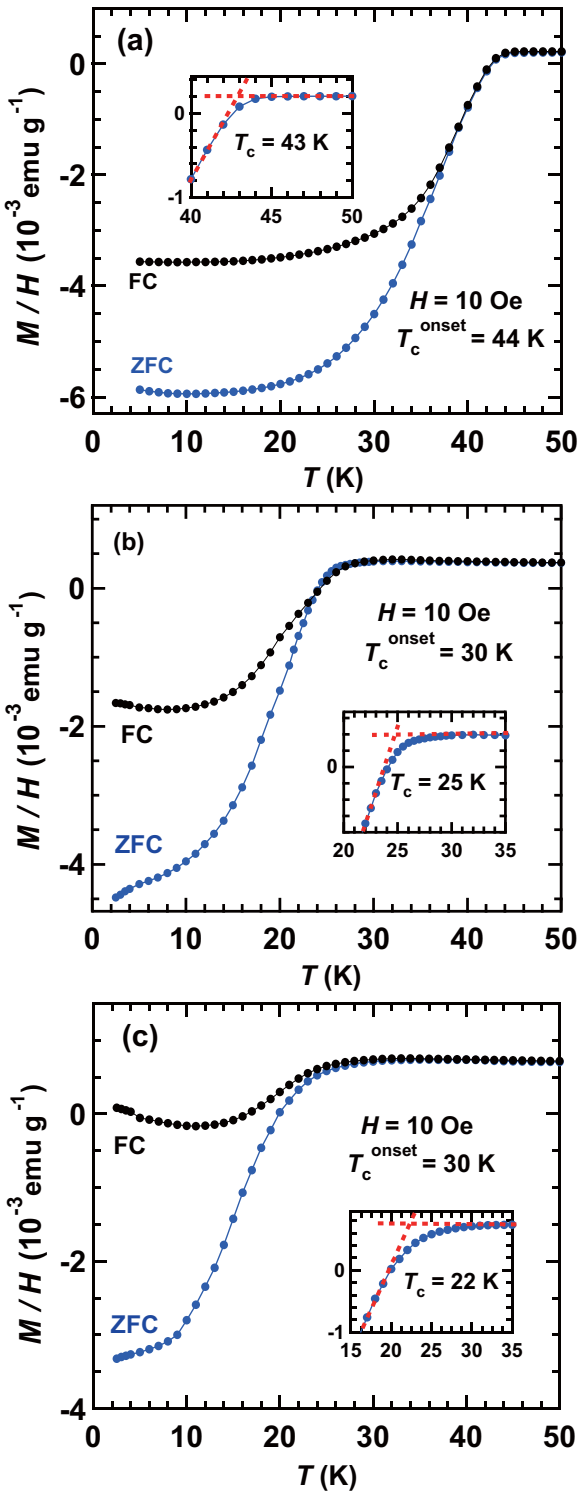

FIG. 2. M/H-T plots measured in ZFC and FC modes for (a) $(EDA)_yNa_xFeSe$; the sample's chemical formula is $(EDA)_yNa_{0.820(7)}Fe_{0.765(1)}Se$. M/H-T plots measured in ZFC and FC modes for (b) high-T_c and (c) low-T_c phases in $(EDA)_yNa_xFeSe_{0.5}Te_{0.5}$; the former's chemical formula is $(EDA)_yNa_{0.8(1)}Fe_{0.88(4)}Se_{0.518(6)}Te_{0.482(6)}$, and the latter's is $(EDA)_yNa_{0.8(2)}Fe_{0.87(5)}Se_{0.51(3)}Te_{0.49(3)}$. Insets of (a)–(c) show how T_c is determined.

$T_c = 45$ K was first generated by Noji *et al.* [16] who provided the plot of T_c against FeSe layer spacing, as described later. The

TABLE I. Superconducting properties, chemical composition, and lattice constants of $(EDA)_yM_xFeSe$ and $(EDA)_yM_xFeSe_{0.5}Te_{0.5}$.

M	Stoichiometry	T_c (K)	T_c^{onset} (K)	a (Å)	c (Å)	SC%[a]
Li	$(EDA)_yLi_xFe_{0.976(1)}Se$	45	46	3.750(3)	22.393(8)	27
Na	$(EDA)_yNa_{0.820(7)}Fe_{0.765(1)}Se$	43	44	3.855(8)	23.50(1)	25
Li	$(EDA)_yLi_xFe_{0.8741(2)}Se_{0.4598(2)}Te_{0.54(5)}$	22.5	26	3.767(2)	22.94(1)	10
Na	$(EDA)_yNa_{0.8(1)}Fe_{0.88(4)}Se_{0.518(6)}Te_{0.482(6)}$	25	30	3.859(3)	22.80(1)	24
Na	$(EDA)_yNa_{0.8(2)}Fe_{0.87(5)}Se_{0.51(3)}Te_{0.49(3)}$	22	30	3.925(3)	24.33(1)	18
K	$(EDA)_yK_{1.17(4)}Fe_{0.83(3)}Se_{0.523(7)}Te_{0.477(7)}$	19	23	3.562(3)	23.57(1)	11

[a]SC refers to shielding fraction. In the evaluation of SC, the density of material was calculated using the above lattice constants and stoichiometry, where density was evaluated by assuming $y = 0.5$ since y is unclear. The y value corresponds to that in $(NH_3)_yM_xFeSe$ and $(NH_3)_yM_xFeSe_{0.5}Te_{0.5}$ [18]. The x of Li was assumed to be 0.5 based on its similarity to Na.

superconducting material $(EDA)_yLi_xFeSe$ was successfully prepared in the present paper, with a T_c of 45 K (Table I).

The EDX spectrum of the $(EDA)_yNa_xFeSe$ sample was measured to determine its stoichiometry and showed only the peaks of Na, Fe, Se, C, N, and O atoms. The O atoms may be present because the sample was exposed to air before the EDX measurement, allowing some oxidation of the sample. This result supports the above chemical formula. The stoichiometry of the sample was determined to be $(EDA)_yNa_{0.820(7)}Fe_{0.765(1)}Se$. The stoichiometries of all $(EDA)_yM_xFeSe$ samples are listed in Table I. Here it should be noted that the low-T_c phase of $(EDA)_yNa_xFeSe$ was prepared, exhibiting a T_c as high as 31 K, but that the shielding fraction was not very high (less than 10%). Consequently, we do not discuss that superconducting phase at the present stage.

The M/H-T plots measured in ZFC and FC modes for $(EDA)_yNa_xFeSe_{0.5}Te_{0.5}$ are shown in Fig. 2(b). The values of T_c^{onset} and T_c were determined to be 30 and 25 K, respectively. The shielding fraction of this sample was 24% at 2.5 K. The T_c is slightly lower than that of the high-T_c phase of $(NH_3)_yNa_xFeSe_{0.5}Te_{0.5}$, which was ~27 K [18]. In the present paper, we successfully prepared another phase of $(EDA)_yNa_xFeSe_{0.5}Te_{0.5}$, i.e., the low-$T_c$ phase. The T_c^{onset} and T_c were 30 and 22 K, respectively, as seen from the M/H-T plots in Fig. 2(c). From the T_c^{onset} value, we must point out that only a small fraction of the high-T_c phase may be contained in this sample. The shielding fraction of this sample was determined to be 18% at 2.5 K.

The EDX spectra of samples containing the high-T_c phase or low-T_c phase of $(EDA)_yNa_xFeSe_{0.5}Te_{0.5}$ were measured to determine their stoichiometry, showing the peaks of Na, Fe, Se, Te, C, N, and O atoms in each sample. The O atom peak may be due to sample exposure to air before the EDX measurement. The EDX spectrum supports the chemical formula of $(EDA)_yNa_xFeSe_{0.5}Te_{0.5}$. The stoichiometry of the sample containing the high-T_c phase of $(EDA)_yNa_xFeSe_{0.5}Te_{0.5}$ was determined to be $(EDA)_yNa_{0.8(1)}Fe_{0.88(4)}Se_{0.518(6)}Te_{0.482(6)}$ and that of the sample containing the low-T_c phase was determined to be $(EDA)_yNa_{0.8(2)}Fe_{0.87(5)}Se_{0.51(3)}Te_{0.49(3)}$.

Furthermore, samples of $(EDA)_yM_xFeSe_{0.5}Te_{0.5}$ (M: Li and K) were also prepared successfully, the T_cs of which were 19–22.5 K (Table I). The T_c of 22.5 K for $(EDA)_yLi_xFeSe_{0.5}Te_{0.5}$ was slightly lower than the T_c (= 26 K) of $(NH_3)_yLi_xFeSe_{0.5}Te_{0.5}$. The T_c^{onset} and T_c for all superconducting phases of $(EDA)_yM_xFeSe_{0.5}Te_{0.5}$ are listed in Table I, along with the stoichiometry of all $(EDA)_yM_xFeSe_{0.5}Te_{0.5}Te_{0.5}$ samples.

The XRD pattern of the high-T_c phase of $(EDA)_yNa_xFeSe_{0.5}Te_{0.5}$ ($T_c = 25$ K) is shown in Fig. 3(a) together with the pattern calculated by Le Bail fitting; the sample's stoichiometry was $(EDA)_yNa_{0.8(1)}Fe_{0.88(4)}Se_{0.518(6)}Te_{0.482(6)}$. Le Bail fitting for the XRD pattern was performed for two phases of $(EDA)_yNa_xFeSe_{0.5}Te_{0.5}$: the high-$T_c$ phase and nondoped $FeSe_{0.5}Te_{0.5}$ in the space group of $I4/mmm$ (No. 139) and $P4/nmm$ (No. 129), respectively. The fraction of the nondoped $FeSe_{0.5}Te_{0.5}$ phase was very small, judging from the XRD pattern [Fig. 3(a)], indicating that the sample's stoichiometry corresponded to that of the high-T_c phase. The final residual pattern factor (R_p) and weighted residual pattern factor (wR_p) were 2.43% and 3.55%, respectively. The a and c of the high-T_c phase were determined to be 3.859(3) and 22.80(1) Å, respectively, while the a and c values of the nondoped phase were 3.910(4) and 5.853(9) Å, which are close to those reported previously for $FeSe_{0.5}Te_{0.5}$: a = 3.7909(5) Å and $c = 5.957(1)$ Å [19]. Since the a and c of $(NH_3)_yNa_xFeSe_{0.5}Te_{0.5}$ (high-T_c phase: $T_c = 30$ K) were 3.874(2) and 19.33(1) Å [18], respectively, c was expanded farther by the insertion of EDA than by NH_3.

The XRD pattern of the low-T_c phase ($T_c = 22$ K) of $(EDA)_yNa_xFeSe_{0.5}Te_{0.5}$ is shown in Fig. 3(b) together with the calculated pattern made by Le Bail fitting; the sample's stoichiometry was $(EDA)_yNa_{0.8(2)}Fe_{0.87(5)}Se_{0.51(3)}Te_{0.49(3)}$. The Le Bail fitting for the XRD pattern was performed for two phases of $(EDA)_yNa_xFeSe_{0.5}Te_{0.5}$: the low-$T_c$ phase and nondoped $FeSe_{0.5}Te_{0.5}$ in the space group of $I4/mmm$ (No. 139) and $P4/nmm$ (No. 129), respectively. The fraction of nondoped $FeSe_{0.5}Te_{0.5}$ was quite small, as shown from the XRD pattern [Fig. 3(b)], indicating that the sample's stoichiometry, $(EDA)_yNa_{0.8(2)}Fe_{0.87(5)}Se_{0.51(3)}Te_{0.49(3)}$, corresponded to that of the low-T_c phase.

The final R_p and wR_p values were 2.8% and 4.2%, respectively. The a and c of $(EDA)_yNa_{0.8(2)}Fe_{0.87(5)}Se_{0.51(3)}Te_{0.49(3)}$ were determined to be 3.925(3) and 24.33(1) Å, respectively, while the a and c values of nondoped $FeSe_{0.5}Te_{0.5}$ were 3.915(6) and 5.88(1) Å, which are also close to those reported previously for $FeSe_{0.5}Te_{0.5}$: a = 3.7909(5) Å and $c = 5.957(1)$ Å [19]. Since the a and c of $(NH_3)_yNa_xFeSe_{0.5}Te_{0.5}$ (low-T_c phase: $T_c = 21$ K) were 3.9824(6) and 17.787(7) Å [18], respectively, the expansion of c was significantly increased by the replacement of NH_3 with EDA. The c

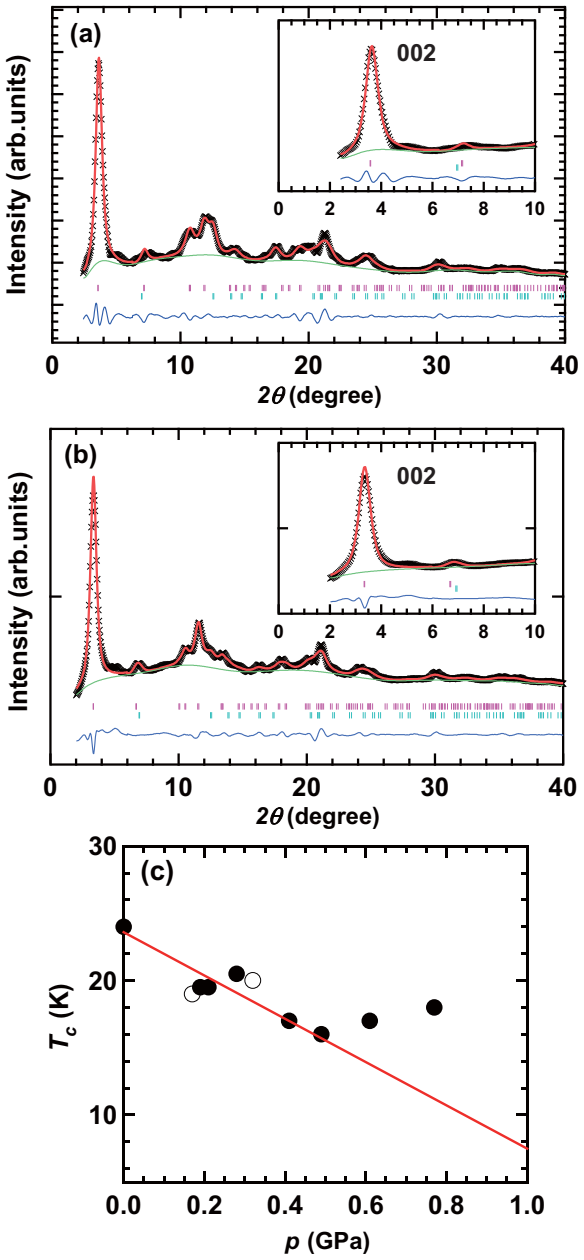

FIG. 3. The XRD patterns (x marks) of (a) high-T_c and (b) low-T_c phases in $(EDA)_yNa_xFeSe_{0.5}Te_{0.5}$; the former sample's chemical formula is $(EDA)_yNa_{0.8(1)}Fe_{0.88(4)}Se_{0.518(6)}Te_{0.482(6)}$, and the latter's is $(EDA)_yNa_{0.8(2)}Fe_{0.87(5)}Se_{0.51(3)}Te_{0.49(3)}$. The red lines in (a) and (b) refer to the calculated XRD patterns from Le Bail fitting. Tick marks indicate the positions of Bragg reflections predicted from lattice constants suggested for the high-T_c phase (top) and β-$FeSe_{0.5}Te_{0.5}$ (bottom) in (a) and for the low-T_c phase (top) and β-$FeSe_{0.5}Te_{0.5}$ (bottom) in (b). (c) Pressure dependence of T_c in the low-T_c phase of $(EDA)_yNa_xFeSe_{0.5}Te_{0.5}$. Solid and open circles refer to data obtained in increasing pressure and decreasing pressure, respectively. The chemical formula is $(EDA)_yNa_{0.6(1)}Fe_{0.85(4)}Se_{0.53(2)}Te_{0.47(2)}$ (T_c = 24 K). The dT_c/dp was determined from the linear relationship (red line).

of 24.33(1) Å in $(EDA)_yNa_{0.8(2)}Fe_{0.87(5)}Se_{0.51(3)}Te_{0.49(3)}$ was also larger than the c of 19.33(1) Å in the high-T_c phase (T_c = 30 K) of $(NH_3)_yNa_xFeSe_{0.5}Te_{0.5}$ [18]. Table I lists the lattice constants of $(EDA)_yM_xFeSe_{0.5}Te_{0.5}$ (M: Li, Na, K). All c values of $(EDA)_yM_xFeSe_{0.5}Te_{0.5}$ are larger than those of $(NH_3)_yM_xFeSe_{0.5}Te_{0.5}$, indicating the co-intercalation of metal atoms and EDA.

The c value of 22.80(1) Å for $(EDA)_yNa_{0.8(1)}Fe_{0.88(4)}Se_{0.518(6)}Te_{0.482(6)}$ (high-T_c phase) is smaller than that of 24.33(1) Å for $(EDA)_yNa_{0.8(2)}Fe_{0.87(5)}Se_{0.51(3)}Te_{0.49(3)}$ (low-T_c phase), showing that the smaller c leads to the higher T_c in $(EDA)_yNa_xFeSe_{0.5}Te_{0.5}$. This result is contrary to that found in $(NH_3)_yNa_xFeSe_{0.5}Te_{0.5}$, as discussed later.

We comment briefly on the orientation of the EDA molecule in the crystal lattice. The EDA molecule must be inserted together with a metal atom in the space between the FeSe ($FeSe_{0.5}Te_{0.5}$) layers in $(EDA)_yM_xFeSe$ [$(EDA)_yM_xFeSe_{0.5}Te_{0.5}$] crystal. As seen from Table I, the c value, 22.94(1) Å, of $(EDA)_yLi_xFeSe_{0.5}Te_{0.5}$ (chemical formula: $(EDA)_yLi_xFe_{0.8741(2)}Se_{0.4598(2)}Te_{0.54(5)}$, T_c = 22.5 K) was larger by 4.965 Å than the 17.975(4) Å of $(NH_3)_yLi_xFeSe_{0.5}Te_{0.5}$ [18]. The van der Waals lengths of the long and short axes of EDA are 7.6 and 5.3 Å, respectively, as seen from Fig. 1. As the expansion (4.965 Å) was smaller than either length, the orientation of the EDA molecule could not be definitely determined.

Figure 3(c) shows the pressure dependence of the M/H–T plot of the low-T_c phase of $(EDA)_yNa_xFeSe_{0.5}Te_{0.5}$. The T_c value decreases with increasing pressure up to 0.5 GPa and slowly increases above 0.5 GPa. The behavior is similar to that of the low-T_c phase of $(NH_3)_yNa_xFeSe_{0.5}Te_{0.5}$ [20], in which the T_c decreases with increasing pressure below 0.5 GPa and saturates above 0.5 GPa. The dT_c/dp for $(EDA)_yNa_{0.6(1)}Fe_{0.85(4)}Se_{0.53(2)}Te_{0.47(2)}$ (T_c = 24 K (low-T_c phase) and a shielding fraction of 10% at 5 K) was determined to be $-16.1(7)\,KGPa^{-1}$ from the linear fitting up to 0.5 GPa [Fig. 3(c)]. The value is similar to that, $-11.7(5)\,KGPa^{-1}$, of the low-T_c phase of $(NH_3)_yNa_{0.4}FeSe_{0.5}Te_{0.5}$ [20]. This result suggests that the change from intercalated NH_3 to EDA does not produce a drastic change in the relationship of T_c and pressure.

Recently, a pressure-induced high-T_c phase was found for $(NH_3)_yCs_xFeSe$ [13], in which the T_c monotonically decreased up to 13 GPa, then rapidly increased to 49 K at 21 GPa. In this paper, we did not investigate the pressure dependence of T_c in such a high pressure range. However, investigating the pressure dependence up to a higher pressure range is very attractive because of the possible emergence of a high-T_c phase. The study of the pressure dependence of $(EDA)_yNa_xFeSe_{0.5}Te_{0.5}$ in the wide pressure range from 0 to 30 GPa is now in progress.

We previously showed a clear correlation between T_c and FeSe plane spacing in $(NH_3)_yM_xFeSe$ [13,18]. The larger the plane spacing becomes in $(NH_3)_yM_xFeSe$, the higher the T_c becomes. Figure 4 shows the T_c as a function of c in M_xFeSe, for which the T_c values were taken from Refs. [9,10,13,16,17] in addition to the data in this paper. The previous T_c-c phase diagram in M_xFeSe was verified by the additional data. Furthermore, the T_c-c phase diagram of $M_xFeSe_{0.5}Te_{0.5}$ (Fig. 4) was depicted using the previous results [18] and the new data; the T_c values of $(EDA)_yM_xFeSe_{0.5}Te_{0.5}$ obtained in this paper are now included in Fig. 4. Both phase diagrams show a dome shape, i.e., the T_c increased with an increase in c (or plane

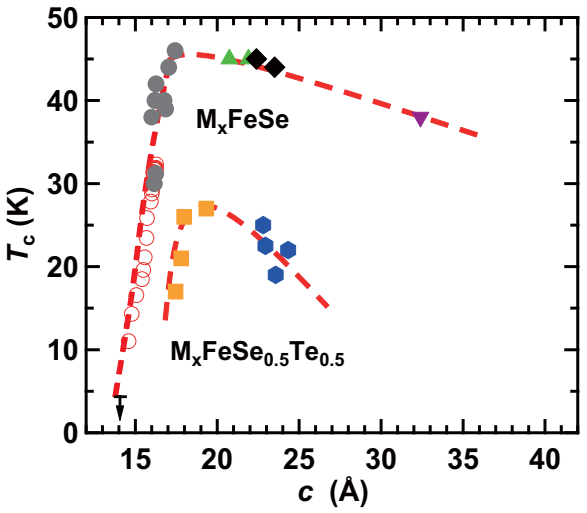

FIG. 4. T_c-c phase diagrams of metal-doped FeSe and metal-doped $FeSe_{0.5}Te_{0.5}$. Eye guides for T_c-c plots are given by dashed lines. Solid circles (gray) refer, respectively, to the T_c values against c for $(NH_3)_yM_xFeSe$ obtained from Refs. [9] and [10]. Open red circles refer to the plots obtained from the pressure dependence of $(NH_3)_yCs_xFeSe$ in Ref. [13]. The solid green triangles refer to the T_c values vs c in $(EDA)_yM_xFeSe$, taken from Ref. [16], and the inverted purple triangles refer to the T_c values vs c of $(HMDA)_yM_xFeSe$ (HMDA: hexamethylenediamine), which are taken from Ref. [17]. The solid orange squares refer to T_c values for $(NH_3)_yM_xFeSe_{0.5}Te_{0.5}$ obtained from Ref. [18]. Solid black diamonds refer to T_c values vs c for $(EDA)_yM_xFeSe$ obtained in this paper, and solid blue hexagons refer to T_c values vs c for $(EDA)_yM_xFeSe_{0.5}Te_{0.5}$ obtained in this paper.

spacing) but the domes decreased slowly as the expansion of plane spacing increased farther. The origin of such a domelike T_c-c phase diagram in metal-doped $FeSe_{1-z}Te_z$ is explained as follows [18]: (i) The increase in 2D nature produces a fundamentally higher T_c, meaning that an increase in Fermi nesting can stabilize the superconducting state and strengthen the electron pairing. (ii) When the $FeSe_{1-z}Te_z$ plane spacing is drastically increased, the T_c saturates or decreases, indicating that interaction between layers is important to the emergence of superconductivity. Thus, the fact that domelike T_c-c behavior is observed in both $M_xFeSe_{1-z}Te_z$ materials with $z = 0$ and $z \neq 0$ is significant evidence for the above scenario. In other words, the domelike T_c-c phase diagram is universal for superconducting $M_xFeSe_{1-z}Te_z$.

IV. CONCLUSIONS AND OUTLOOK

For this paper, we prepared superconducting metal-doped FeSe and $FeSe_{0.5}Te_{0.5}$, $(EDA)_yM_xFeSe$ and $(EDA)_yM_xFeSe_{0.5}Te_{0.5}$, using an organic solvent, EDA. These superconductors enabled us to make a precise T_c-c phase diagram for M_xFeSe and $M_xFeSe_{0.5}Te_{0.5}$, showing that larger c (or layer spacing) leads to higher T_c, but an extreme expansion of c suppresses the T_c. This implies the importance of valance of Fermi nesting and layer interaction in metal-doped $FeSe_{1-z}Te_z$ materials, i.e., the optimal c for the superconductivity exists. The further expansion of c using other organic solvents is now in progress. We also investigated the pressure dependence of T_c in $(EDA)_yNa_xFeSe_{0.5}Te_{0.5}$ at 0–0.8 GPa. This paper may proceed to the observation of pressure-driven high-T_c superconductivity, which has already been confirmed in $(NH_3)_yCs_xFeSe$ at the pressure greater than 15 GPa [13] and K_xFeSe at the pressure more than 10 GPa [8].

ACKNOWLEDGMENTS

The authors especially thank Prof. Hideki Okamoto of Okayama University for his valuable suggestion about the EDA molecule. This paper was partly supported by Grants-in-Aid No. 26105004 and No. 26400361 from Ministry of Education, Culture, Sports, Science, and Technology (MEXT). This paper was also supported by JST ACT-C Grant No. JPMJCR12YW, Japan, and by the Program for Promoting the Enhancement of Research Universities.

[1] Y. Kamihara, T. Watanabe, M. Hirano, and H. Hosono, J. Am. Chem. Soc. **130**, 3296 (2008).
[2] H. Takahashi, K. Igawa, K. Arii, Y. Kamihara, M. Hirano, and H. Hosono, Nature **453**, 376 (2008).
[3] M. Rotter, M. Tegel, and D. Johrendt, Phys. Rev. Lett. **101**, 107006 (2008).
[4] J. H. Tapp, Z. J. Tang, B. Lv, K. Sasmal, B. Lorenz, P. C. W. Chu, and A. M. Guloy, Phys. Rev. B **78**, 060505(R) (2008).
[5] Z.-A. Ren, G.-C. Che, X.-L. Dong, J. Yang, W. Lu, W. Yi, X. L. Shen, Z.-C. Li, L.-L. Sun, and F. Zhou, Europhys. Lett. **83**, 17002 (2008).
[6] F.-C. Hsu, J.-Y. Luo, K.-W. Yeh, T.-K. Chen, T.-W. Huang, P. M. Wu, Y.-C. Lee, Y.-L. Huang, Y.-Y. Chu, D.-C. Yan, and M.-K. Wu, Proc. Natl. Acad. Sci. USA **105**, 14262 (2008).
[7] J. G. Guo, S. F. Jin, G. Wang, S. C. Wang, K. X. Zhu, T. T. Zhou, M. He, and X. L. Chen, Phys. Rev. B **82**, 180520(R) (2010).
[8] L. L. Sun, X.-J. Chen, J. Guo, P. W. Gao, Q.-Z. Huang, H. D. Wang, M. H. Fang, X. L. Chen, G. F. Chen, Q. Wu, C. Zhang, D. C. Gu, X. L. Dong, L. Wang, K. Yang, A. G. Li, X. Dai, H.-K. Mao, and Z. X. Zhao, Nature **483**, 67 (2012).
[9] T. P. Ying, X. L. Chen, G. Wang, S. F. Jin, T. T. Zhou, X. F. Lai, H. Zhang, and W. Y. Wang, Sci. Rep. **2**, 426 (2012).
[10] L. Zheng, M. Izumi, Y. Sakai, R. Eguchi, H. Goto, Y. Takabayashi, T. Kambe, T. Onji, S. Araki, T. C. Kobayashi, J. Kim, A. Fujiwara, and Y. Kubozono, Phys. Rev. B **88**, 094521 (2013).
[11] T. P. Ying, X. L. Chen, G. Wang, S. F. Jin, X. F. Lai, T. T. Zhou, H. Zhang, S. J. Shen, and W. Y. Wang, J. Am. Chem. Soc. **135**, 2951 (2013).
[12] L. Zheng, X. Miao, Y. Sakai, M. Izumi, H. Goto, S. Nishiyama, E. Uesugi, Y. Kasahara, Y. Iwasa, and Y. Kubozono, Sci. Rep. **5**, 12774 (2015).
[13] M. Izumi, L. Zheng, Y. Sakai, H. Goto, M. Sakata, Y. Nakamoto, H. L. T. Nguyen, T. Kagayama, K. Shimizu, S. Araki, T. C. Kobayashi, T. Kambe, D. C. Gu, J. Guo, J. Liu, Y. C. Li, L. L. Sun, K. Prassides, and Y. Kubozono, Sci. Rep. **5**, 9477 (2015).

[14] M. Burrard-Lucas, D. G. Free, S. J. Sedlmaier, J. D. Wright, S. J. Cassidy, Y. Hara, A. J. Corkett, T. Lancaster, P. J. Baker, S. J. Blundell, and S. J. Clarke, Nat. Mater. **12**, 15 (2013).
[15] T. Hatakeda, T. Noji, T. Kawamata, M. Kato, and Y. Koike, J. Phys. Soc. Jpn. **82**, 123705 (2013).
[16] T. Noji, T. Hatakeda, S. Hosono, T. Kawamata, M. Kato, and Y. Koike, Physica C **504**, 8 (2014).
[17] S. Hosono, T. Noji, T. Hatakeda, T. Kawamata, M. Kato, and Y. Koike, J. Phys. Soc. Jpn. **83**, 113704 (2014).
[18] L. Zheng, Y. Sakai, X. Miao, S. Nishiyama, T. Terao, R. Eguchi, H. Goto, and Y. Kubozono, Phys. Rev. B **94**, 174505 (2016).
[19] Y. Mizuguchi, F. Tomioka, S. Tsuda, T. Yamaguchi, and Y. Takano, J. Phys. Soc. Jpn. **78**, 074712 (2009).
[20] Y. Sakai, L. Zheng, M. Izumi, K. Teranishi, R. Eguchi, H. Goto, T. Onji, S. Araki, T. C. Kobayashi, and Y. Kubozono, Phys. Rev. B **89**, 144509 (2014).